Release of Oxygen Atoms and Nitric Oxide Molecules from the Ultraviolet Photodissociation of Nitrate Adsorbed on Water Ice Films at 100 K

Akihiro Yabushita, Noboru Kawanaka, and Masahiro Kawasaki*

Department of Molecular Engineering, Kyoto University, Kyoto 615-8510, Japan

Paul D. Hamer and Dudley E. Shallcross*

Bristol Biogeochemistry Research Centre, School of Chemistry, University of Bristol, Bristol BS8 1TS, United Kingdom

Received: April 3, 2007; In Final Form: June 1, 2007

Production of $O(^3P_J, J = 2, 1, 0)$ atoms from the 295−320 nm photodissociation of NO_3^- adsorbed on water polycrystalline ice films at 100 K was directly confirmed using the resonance-enhanced multiphoton ionization technique. Detection of the O atom signals required an induction period after deposition of HNO_3 onto the ice film held at 130 K due to the slow ionization rate of HNO_3 to H^+ and NO_3^- with a rate constant of $k = (5.3 \pm 0.2) \times 10^{-3}$ s^{-1}. Translational energy distributions of the O atoms were represented by a combination of two Maxwell−Boltzmann energy distributions with translational temperatures of 2000 and 100 K. Direct detection of NO from the secondary photodissociation process was also successful. On the atmospheric implications, the influence of the direct release of the oxygen atoms into the air from NO_3^- adsorbed on the natural snowpack was included in an atmospheric model calculation on the mixing ratios of ozone and nitric oxide at the South Pole, and the results compared favorably with the field data.

Introduction

An aqueous solution of nitric acid, a strong oxidizing reagent, generates oxygen molecules when it is irradiated by ultraviolet light because the photolysis of the aqueous nitrate at wavelengths (λ) > 300 nm and under pH < 6 in fluid or frozen media proceeds via two channels:

	ΔH kJ mol^{-1}	λ_{th} nm	
$NO_3^-(d) + h\nu \rightarrow O(^3P)(g) + NO_2^-(d)$	352	340	(1)
$NO_3^-(d) + h\nu \rightarrow O^-(d) + NO_2(g)$	190	630	(2)

where λ_{th} stands for the threshold wavelength, 'd' for dilute solution, and 'g' for gas phase.[1] Previous laboratory studies concerning the photolysis of NO_3^- have demonstrated that the reaction proceeds via reactions 1 and 2 using laser-induced fluorescence techniques for NO_2,[2,3] or based on product analysis using an benzoic acid scavenger[4] and an oxygen-atom scavenger.[5] Generation of oxygen atoms from the photolysis of NO_3^- in an aqueous solution was indirectly confirmed by the radical scavenging technique with cyclopentene by probing the production of ethane.[5−7] However, direct observation of oxygen atom release from the ultraviolet photodissociation of NO_3^- has not been performed.

Referred to as "snowpack photochemistry", the summertime atmospheric boundary layer over the South Pole is highly oxidizing with unexpectedly high levels of NO_x, OH, and O_3.[8] Nitrate plays a crucial role in the snowpack acting as a source of NO_x and OH radicals[9] because the nitrite formed in reaction 1 and NO_2 formed in reaction 2 undergo further photodissociation:

in snowpack

$$NO_2^- + h\nu\ (+ H^+) \rightarrow NO + OH/HONO \quad (3)$$

in the gas phase

$$NO_2 + h\nu \rightarrow NO + O(^3P) \quad (4)$$

The NO_x production and release to the gas phase as a result of the ultraviolet radiation impacting onto NO_3^- dissolved in ice have been observed in several laboratory studies[2,10,11]

In this work, we focused on direct detection of the oxygen atom via reaction 1 from the ultraviolet photodissociation of NO_3^- adsorbed on a water ice film using laser ionization time-of-flight (TOF) techniques. The secondary photoproduct NO via reaction 3 was also investigated. If direct release of O atoms and NO molecules is confirmed, the O_3 and NO_x production via reactions 1, 3, and 4 will have a large impact on the origins of the air pollution at the South Pole.[12]

Experimental Details

1.Time-of-Flight Apparatus and Preparation of Ice Films. The experimental apparatus used in the present study has been described previously.[13] A vacuum chamber was evacuated to a base pressure of 10^{-8} Torr using two turbo-molecular pumps in tandem (Mitsubishi Heavy Industry, 800 and 50 L s^{-1}). An optically flat sapphire substrate, sputter coated with a thin film of Au, was supported in the center of the chamber by a liquid-nitrogen-cooled manipulator connected to an *X*-*Y*-*Z* stage.[14] The temperature of the substrate was controlled to within 1 K. The controller was composed of an alumel−chromel resistance thermometer with cooling, by liquid nitrogen, and heating from

* Corresponding authors. E-mail: (M.K.) kawasaki@photon.mbox.media.kyoto-u.ac.jp; (D.E.S.) d.e.shallcross@bris.ac.uk. Fax: (M.K.) +81-75-383-2573; (D.E.S.) +44−117-9250612.

10.1021/jp072596j CCC: $37.00 © 2007 American Chemical Society
Published on Web 08/16/2007

a 0.35 mm diameter tantalum filament attached to the substrate. Polycrystalline ice (PCI) films were prepared with the backfilling deposition of water vapor onto the substrate at 130 K for 60 min by a pulsed nozzle (General Valve) at a rate of 10 Hz, at a 45° incidence angle, and at 20 Torr stagnation pressure of water vapor and then maintained at this temperature for a further 30 min for annealing purposes. The exposure of H_2O was typically 1800 L (1 L = 1×10^{-6} Torr s), which resulted in the formation of 600 mL of H_2O on the Au substrate.[15]

Commercially available nitric acid (69%) was dried in a glass container with concentrated sulfuric acid (97%) to remove water. The gas mixture of HNO_3 (approximately 30 Torr) with N_2 diluent (approximately 730 Torr) was introduced into a vacuum chamber with the backfilling method by a pulsed nozzle. The exposure of HNO_3 was typically 2 L (1 L = 1×10^{-6} Torr s) on the PCI film for 10 min duration at 130 K, and the substrate temperature was held at 130 K for up to 90 min. A sticking (uptake) coefficient is reported to be 0.3.[16] After the substrate temperature was reduced to 100 K, UV photoirradiation and resonance-enhanced multiphoton ionization (REMPI) detection of O atoms were performed. The ice film thus dosed was photodissociated at 295−320 nm with a YAG pumped dye laser (Lambda Physik, SCANmate, 1 mJ cm^{-2} $pulse^{-1}$ at UV). Another YAG pumped dye laser pulse (1 mJ $pulse^{-1}$ at UV) was used to ionize the photofragments by the (2 + 1) REMPI transition of $O(^3D_J-{}^3P_2)$ at 225.72 nm with a lens (f = 0.10 m). The subsequent REMPI signals were detected by a time-of-flight mass spectrometer and normalized to the UV probe laser intensity. The distance, r, between the substrate and the detection region was varied from 2 to 5 mm to change the effective flight lengths for neutral $O(^3P_J)$ atom photofragments, which were set typically to 2 mm. REMPI signal intensities were taken as a function of time delay, t, between the photolysis and probe laser pulses, which correspond to the flight time between the substrate and the REMPI detection region. Nitric oxide was probed by the (2 + 1) REMPI transition of NO-$(A^2\Sigma-{}^2\Pi, 0-0, J'')$ at 225.6−226.4 nm.

2. Simulation of Time-of-Flight Spectra of O Atoms. The TOF spectra were fitted with $S(t, T_1, T_2, T_3)$, consisting of three flux-weighted Maxwell−Boltzmann (MB) distributions $P_{M-B}(E_t, T_{trans})$, defined by translational temperatures T_i, and coefficient, a_i,

$$S(a_i, t, T_1, T_2) = a_1 S_{MB}(t, T_1) + a_2 S_{MB}(t, T_2) + (1 - a_1 - a_2) S_{MB}(t, T_3) \quad (5)$$

$$S_{MB}(t, r) = r^3 t^{-4} \exp[-mr^2/(2k_B T_{trans} t^2)] \quad (6)$$

$$P_{MB}(E_t, T_{trans}) = (k_B T_{trans})^{-2} E_t \exp[-E_t/(k_B T_{trans})] \quad (7)$$

where r is a flight length for the photofragment. $P_{MB}(E_t, T_{trans})$ is characterized by the average translational energy $\langle E_t \rangle = 2k_B T_{trans}$, where k_B is the Boltzmann constant. Since the ice films employed in these experiments were of polycrystalline surface morphology, the angular distributions of the O atoms were all assumed to be isotropic. The accuracy of the conversion procedure was confirmed experimentally by changing the flight length from 2 to 5 mm with the aid of the *X*-*Y*-*Z* stage. The effective irradiated area was determined by a round slit of 10 mm diameter. This size is the part of the film on the substrate.

The details of the simulation for the TOF spectra were described in our previous paper.[13] The conversion procedure was described by Zimmermann and Ho.[17]

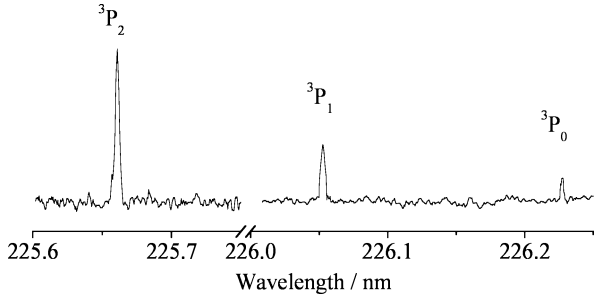

Figure 1. REMPI excitation spectrum of $O(^3P_J)$ from the 305 nm photodissociation of NO_3^- on a polycrystalline water ice film. The substrate temperature was 100 K at 2 μs time-of-flight.

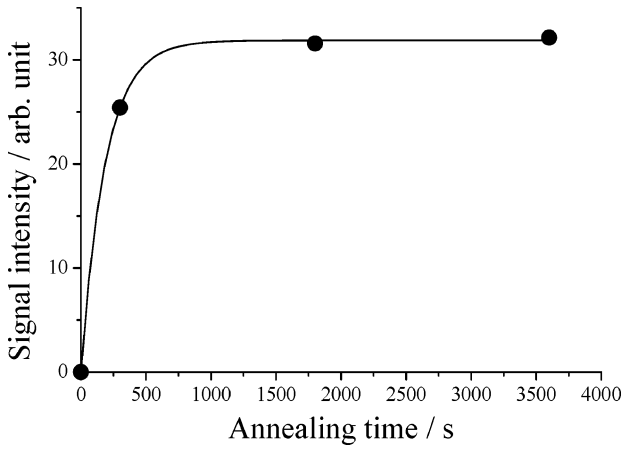

Figure 2. Time evolution of $O(^3P_2)$ signal intensity after deposition of HNO_3 on the ice film at 130 K at 2 μs time-of-flight. During the intercept of measurement, the UV photodissociation beam at 305 nm was blocked. The measured evolution curve is fitted to a single-exponential curve with a rate constant of $(5.3 \pm 0.2) \times 10^{-3}$ s^{-1}.

Results

1. Resonance-Enhanced Multiphoton Ionization Detection of $O(^3P_J)$ Atoms. 1.1. Excitation Spectrum and Temporal Evolution of O Atom Signal Intensity. Figure 1 shows the REMPI spectrum for the spin−orbit levels of $O(^3P_J)$ from the 305 nm photodissociation, 30 min after deposition of HNO_3 to a PCI film at 130 K. The delay between photolysis and probe laser pulse was 2 μs. Three different levels were generated. The signal intensity of $O(^3P_2)$ was measured as a function of annealing time at 130 K after deposition of HNO_3. No REMPI signals were detected just after deposition of HNO_3 since the dissolution and ionization of HNO_3 into H^+ and NO_3^- on the PCI film surface is a slow process, on the order of 10 min.[18] The measured evolution curve in Figure 2 can be fitted to a single-exponential curve with a rate constant of $(5.3 \pm 0.2) \times 10^{-3}$ s^{-1}. During the intercept of this measurement, the photodissociation laser pulse at 305 nm was blocked. Detection of $O(^3P_2)$ atoms was also successful from the photodissociation at 295 and 320 nm.

The temporal decay of the $O(^3P_2)$ signal intensity was measured as a function of UV irradiation time. The signal intensity decreased with a time constant of 1/10 min^{-1}.

1.2. Translational Temperatures of $O(^3P_2)$ Atoms. Figure 3 shows a TOF spectrum of the $O(^3P_2)$ atoms from the 305 nm photodissociation at 30 min after deposition of HNO_3 on a PCI film at 130 K. After the substrate temperature was reduced to 100 K, the TOF spectrum was measured, which is well reproduced by summing three different MB distributions: the component A with $T_{trans} = 2000 \pm 200$ K contributing 48 ± 4%, the component B with $T_{trans} = 500 \pm 50$ K contributing 11 ± 4%,

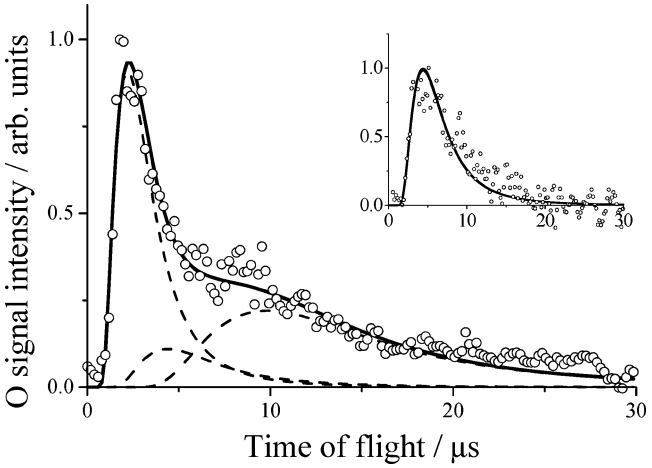

Figure 3. Typical time-of-flight spectrum of REMPI signals of $O(^3P_2)$ atoms from the photodissociation of NO_3^- on a polycrystalline water ice film at 305 nm. The measurement was undertaken at the substrate temperature of 100 K. The solid lines are fits to the data derived assuming three Maxwell−Boltzmann distributions, $T = 2000$ K for the fast component, 500 K for the middle one, and 100 K for the slow one. The inset shows time-of-flight spectrum of $O(^3P_2)$ atoms from the photodissociation of NO_2 on water ice films at 305 nm. The solid line is a fit to the data derived assuming Maxwell−Boltzmann distribution with $T = 500$ K.

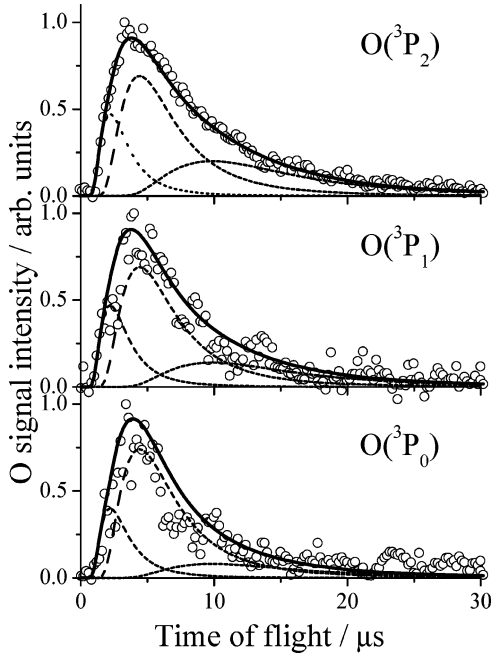

Figure 4. Time-of-flight spectra of REMPI signals of O (^3P_J, $J = 0$, 1, 2) atoms from the photodissociation of NO_3^- on a polycrystalline water ice film at 305 nm after prolonged UV irradiation for O ($^3P_2$), or just after deposition for O ($^3P_1$) and O ($^3P_0$). The measurement was undertaken at the substrate temperature of 100 K. The solid lines are fits to the data derived assuming three Maxwell−Boltzmann distributions, $T = 2000$ K for the fast component, 500 K for the middle one, and 100 K for the slow one.

and the component C with $T_{trans} = 100 \pm 10$ K contributing 41 ± 8%. The inset shows a TOF spectrum of $O(^3P_2)$ atoms from the 305 nm photodissociation of NO_2 adsorbed on a PCI film at 100 K. This TOF spectrum is reproduced by a single component B with 500 ± 50 K in the M−B distribution.

The TOF spectra were also obtained for $O(^3P_0)$ and $O(^3P_1)$, which consist mostly of component B. Similarly after prolonged irradiation of the UV dissociation laser pulses for 60 min, the TOF spectrum of $O(^3P_2)$ changed to consist mainly of component B. These spectra are shown in Figure 4.

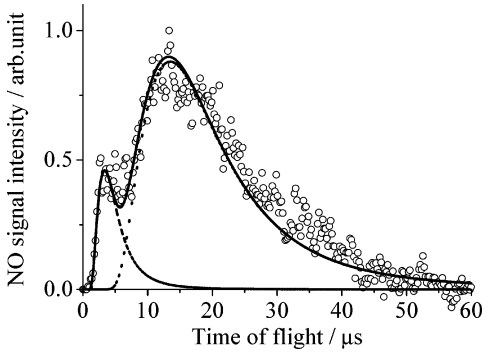

Figure 5. Time-of-flight spectrum of REMPI signals of NO (Q branch) at 226.25 nm from the photodissociation of NO_3^- on a polycrystalline water ice film at 305 nm. The measurement was undertaken at the substrate temperature of 100 K. The solid lines are fits to the data derived assuming two Maxwell−Boltzmann distributions, $T = 1600$ K for the fast component and 100 K for the slow one.

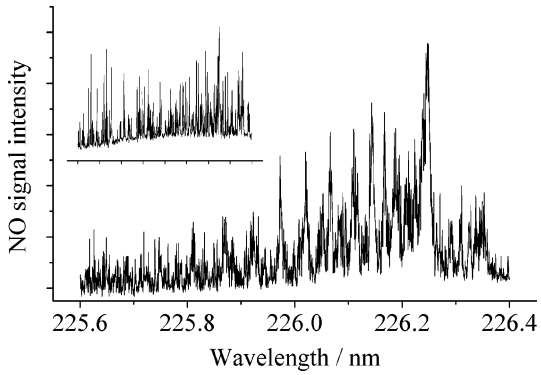

Figure 6. REMPI excitation spectrum of NO(A−X, 0−0) from the photodissociation of NO_3^- on a polycrystalline water ice film. The substrate temperature is 100 K, and the time-of-flight is 15 μs. The inset shows the spectrum at time-of-flight = 5 μs.

We also performed the photodissociation at 193 nm just after deposition of HNO_3 on the ice film. The REMPI TOF spectrum of $O(^3P_2)$ at 193 nm was fitted by $T_{trans} = 2300 \pm 200$ K contributing 46 ± 3% and $T_{trans} = 130 \pm 20$ K contributing 54 ± 3%.

2. Resonance-Enhanced Multiphoton Ionization Detection of Nitric Oxide. Figure 5 shows a time-of-flight spectrum of REMPI signals of NO (Q branch) at 226.25 nm from the photodissociation of NO_3^- on a polycrystalline water ice film at 305 nm. The film surface was kept at 130 K for 30 min after deposition of HNO_3 on a PCI film at 130 K. The measurement was undertaken at the substrate temperature of 100 K. The solid lines are fits to the data derived assuming two Maxwell−Boltzmann distributions, $T = 1600$ K for the fast component with contribution of 19% and 100 K for the slow one.

Figure 6 shows the REMPI spectra of NO. The delay between photolysis and probe laser pulse was 5 and 15 μs. The rotational temperature of NO is higher than the substrate temperature. The faster NO photofragment is more rotationally excited than the slower one, which is common in surface photodissociation.[19,20] We did not try to probe NO_2 from reaction 2 because of low sensitivity of the REMPI technique to NO_2.[2]

Discussion

1. Origin of O Atoms from the UV Photodissociation. Dissociation processes of HNO_3 into ice film surfaces occur via dissolution followed by ionization:

	ΔH kJ mol^{-1}	
$HNO_3(l) + H_2O(l) \rightarrow HNO_3 \cdot H_2O(l)$	−14	(8)
$HNO_3(l) + 3H_2O(l) \rightarrow HNO_3 \cdot 3H_2O(l)$	−25	(9)
$HNO_3 \cdot H_2O(l) \rightarrow H_3O^+(d) + NO_3^-(d)$	−20	(10)
$HNO_3 \cdot 3H_2O(l) \rightarrow H_3O^+(d) + NO_3^-(d) + 2H_2O(l)$	−10	(11)

Pursell et al. examined the ionization process of HNO_3 into $H^+ + NO_3^-$ on water ice films using FTIR transmission spectroscopy.[18] They found that the ionization rate constant of HNO_3 into the ice surface layer is $k = (4.9 \pm 0.7) \times 10^{-3}$ s^{-1} and found no apparent temperature dependence at 130−150 K. The activation energy of the ionzation process is reported to be 0 ± 8 kJ mol^{-1}.[18] The present evolution time constant of $(5.3 \pm 0.2) \times 10^{-3}$ s^{-1} at 130 K for the O atom signal is in agreement with the reported ionization rate constant of HNO_3 at 130−150 K.

Assuming that the NO_3^- diffusion in the ice surface layer may be comparable to the measured diffusion of HNO_3 in ice,[21] the dissociation (ionization) constant may be calculated. Using a value extrapolated to 130 K and assuming an average distance of 1−2 bilayers of water (approximately 0.36−0.73 nm), the calculated rate constant is $(4.3-18) \times 10^{-6}$ s^{-1}. This mobility constant of NO_3^- in the ice film is much smaller than our experimentally determined time constant. The change of the TOF spectra after extensive UV irradiation supports the surface NO_3^- photodissociation because the supply of NO_3^- to the ice surface is not fast enough.

The TOF spectrum of the O($^3P_2$) atoms in Figure 3 consists of the fast, middle, and slow components. The fast component A comes from the photodissociation of NO_3^-. The slow component C that corresponds to 100 K in the M−B distribution is accommodated by the ice bulk at 100 K. The accommodation of the photofragments by the bulk phase was also reported (a) for H atoms from the photodissociation of bulk ice water films[22] and (b) for NO from the photodissociation of $NO_2(N_2O_4)$ adsorbed on water films.[23] The translational temperature of the residual middle component B corresponds to the component from the photodissociation of NO_2 at 305 nm (the inset of Figure 3). Thus, it is tempting to associate the component B with photodissociation of NO_2 sequentially formed from the UV photodissociation of NO_3^-. If NO is produced from NO_2 in the gas phase, NO would be highly rotationally excited at both 5 and 15 μs times-of-flight (delay between dissociation and probe laser pulses) because the large excess energy is as large as ca. 8000 cm^{-1} and NO_2 is bent. These considerations suggest that NO is produced via the sequential processes via reaction 1 followed by reaction 3. Since the photoabsorption cross section of NO_2^- on a water ice film is 3.2×10^{-20} cm,[2,24] this secondary dissociation could proceed very quickly.[25] The TOF spectrum of O($^3P_2$) in Figure 4 is further evidence that NO_2 was photoprepared on the ice surface since, after prolonged UV irradiation, the TOF component consists mainly of the component B that is clearly observed from the photodissociation of NO_2 adsorbed on the ice surface. NO is the product of secondary photolysis, reaction 3; an induction period would be anticipated for the NO signal to rise to detectable levels.[26,27]

It should be noted that O($^3P_0$) and O($^3P_1$) are produced from the secondary photoprocess via NO_2 based on the TOF data in Figure 4. However, the spin−orbit branching ratio in Figure 1 reflects the nascent one because the measured TOF components were the component A. Warneck and Wurzinger[6] reported the quantum yields at 305 nm for reactions 1 and 2 in aqueous solution to be 1.1×10^{-3} and 9.2×10^{-3}, respectively. Bartels-Rausch and Donaldson[28] reported the NO_2 and HONO release in the snowpack photochemistry. NO_2 release was not affected by temperature changes in the range of 193 and 253 K. A HONO quantum yield of $(3.8 \pm 0.6 \times 10^{-4})$ is approximately 1 order of magnitude lower than the reported quantum yield for NO_2 formation.

As the other source of O atoms, the photodissociation processes of HNO_3 are thermodynamically possible.

	ΔH kJ mol^{-1}	λ_{th} nm	
$HNO_3(d) + h\nu \rightarrow O(^3P)(g) + HONO(g)$	377	317	(12)
$HNO_3(d) + h\nu \rightarrow OH(g) + NO_2(g)$	280	427	(13)

Since the absorption cross section of HNO_3 in the gas phase is 1×10^{-17} cm^2 at 193 nm, the O atom production via reaction 12 is open. However at 305 nm, no signal appeared just after deposition of HNO_3. The gas phase absorption cross section is 2.4×10^{-21} cm^2 around 300 nm. Probably the absorption spectrum is blue-shifted on a cold ice film. The other possible reason might be the low quantum yield of the O atom formation. Using excitation at 266 nm in the gas phase, Margitan and Watson found the quantum yield of O atoms to be 0.031 ± 0.010.[29] Recently, the quantum yield for OH formation from the photolysis of HNO_3 via reaction 13 was measured to be 1.05 ± 0.29 at 308 nm.[30]

2. Atmospheric Implications. The influence of the direct release of the oxygen atoms into the atmosphere from NO_3^- adsorbed on ice surfaces has potential implications for the formation of ozone and the cycling of NO_x species in the Arctic and Antarctic boundary layer and in the upper troposphere impacted by cirrus clouds. The Antarctic boundary layer has been shown to contain elevated levels of NO_x[8,31−33] that are generated from snowpack photochemistry of nitrate.[11,34,35]

High ozone levels have also been observed at the South Pole during summer,[36] where levels of NO_x were also elevated (50−600 parts per trillion).[32] However, observed levels of reactive non-methane hydrocarbons are extremely low (typically a few ppt), too low in fact to support significant ozone production. A recent modeling study[37] has shown that oxygenated VOCs (OVOCs) are important for the production of elevated levels of ozone at the South Pole in the absence of appreciable levels of non-methane hydrocarbons. Even with this OVOC enhancement, the model cannot reproduce the highest levels of ozone (45 ppb), even with the highest levels of observed OVOCs (e.g., CH_3OOH). The South Pole Antarctic Boundary Layer Model used in the described study[37] has been re-run to include photoproduction of O atoms from nitrate by adding a flux from reaction 1 of O atoms relative to the observationally derived flux of NO derived from NO_2^- photolysis.[38]

Snow and ice found in the polar region where the temperatures are substantially higher than the present condition (100 K) and where the quasi-liquid layers on ice and snow at $T >$ 200 K may play a very important role in mediating the reaction pathways. We assume that the photolysis products of nitrate dissolved on the surface of the quasi-liquid layer would be no different from the observations in liquid phase. The quantum yield of O atom release at around 300 nm is estimated to be on the order of $(1-10) \times 10^{-3}$. The release of the O atom from the surface photolysis would not be affected by the presence of the liquid. Hence, we would consider that in both systems (solid and quasi-liquid phases) the surface nitrate photolysis is leading to gas-phase release of O atoms. Figure 7 shows the result of model runs (lines) where the flux from the surface of O atoms

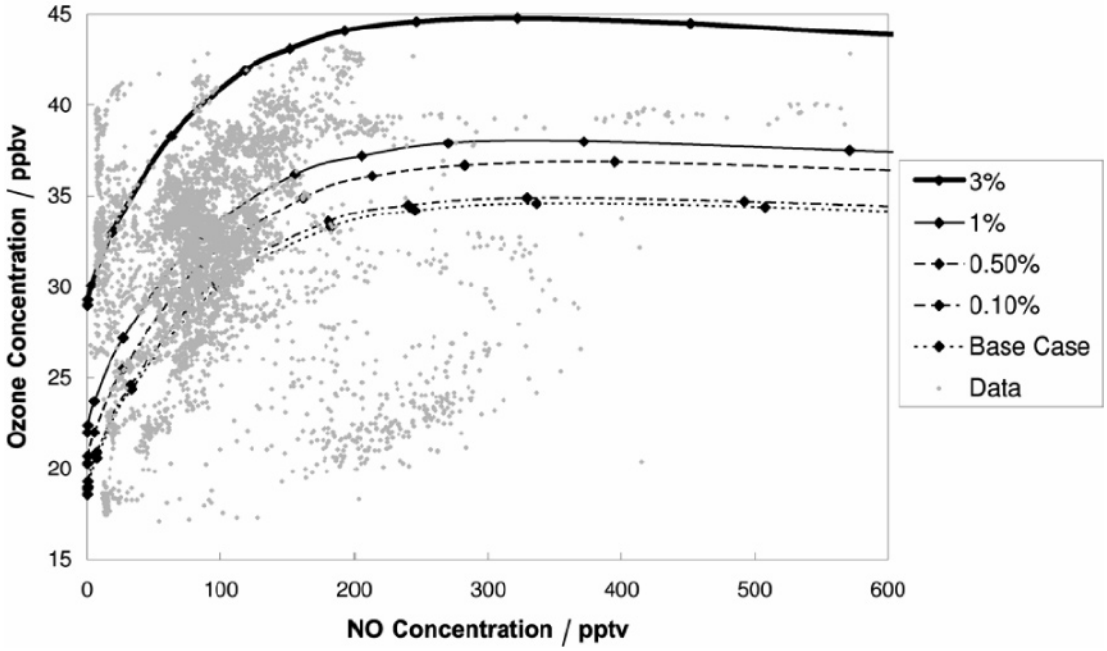

Figure 7. Levels of O_3 as a function of specific NO concentrations. Result of model runs (lines) where the flux from the surface of O atoms is included. These model runs are compared with measurement data of O_3 and NO at the South Pole (gray points).

relative to the observed NO emission was increased. Such an increase leads to elevated levels of O_3 for specific NO concentrations. These model runs are compared with measurement data of O_3 and NO from the South Pole (gray points). The results for the oxygen atom quantum yield of 0.5−1.0% are in agreement with the field measurement data. The very high levels of ozone observed at NO levels less than around 20 ppt are believed to be caused due to the rather sudden development of a very deep boundary layer on the plateau. During such events ozone is typically mixed up from the surface to elevations in excess of 500 m so it does not change in concentration at the same rate that NO does.[39] It is clear that in order to reproduce the highest levels of ozone observed, at NO levels between 100 and 600 ppt, a flux of O atoms that is about 3% of that of NO is required, and this flux encompasses most of the measurement data. Without this additional mechanism it is impossible to reconcile this model with measurements, and it would seem that this is a vital missing piece of the puzzle at the South Pole.

A major focus in atmospheric science has been on understanding the annual springtime increase in ozone. Ozone lidar data collected from February to May 2000 between Colorado (United States) and northern Canada and Greenland as part of the Tropospheric Ozone Production about the Spring Equinox (TOPSE) airborne campaign clearly show this transition throughout the free troposphere.[40] Analysis of odd nitrogen (NO_y) and its constituents confirmed previous ground-based studies showing that, as temperatures warm, thermal decomposition of peroxy acetyl nitrate (PAN) is the primary driving factor, leading to enhanced photochemical ozone production from released NO_x.[41,42]

The springtime breakdown of the Arctic haze's pollution reservoir and its subsequent southward transport may also contribute to spring ozone maxima observed at remote mountain sites in Northern mid-latitudes.[43,44] However, inconsistencies were found between observations and model calculations of oxygenated organic and nitrogen-containing species, e.g., nitrous acid (HONO), pernitric acid (HNO_4), and PAN,[45] and also, more recently in hydroxyl radical (OH) data collected at the high-altitude Summit site in Greenland (38.4° W, 72.6° N, 3208 m ASL)[46] suggesting that our knowledge of Arctic photochemistry and processes, such as wet scavenging, is incomplete. The summertime ozone budget has yet to be quantified in the Arctic. Although not explicitly modeled in this study, we surmise that the impact of O atom production from snowpack photolysis will go some way to reconciling these discrepancies in the Arctic. However, there still remains a discrepancy between measured and modeled ratios of NO_x to NO_y. Models consistently overpredict HNO_3 concentrations, and hence NO_y, and tend to underpredict NO_x. This suggests that nitrate photolysis is occurring within this atmospheric region and that the NO_3^- photolysis mechanism will redress this discrepancy and ultimately lead to enhanced ozone formation. Further work is required to determine whether this mechanism has a significant impact on the upper free troposphere.

Conclusion

Direct release of $O(^3P_J)$ atoms from the photodissociation of NO_3^- adsorbed on water ice films at 100 K was confirmed in the solar UV radiation region. This finding could provide a new production pathway of ozone in the mechanism for the snowpack photochemistry in the Arctic at the South Pole. After prolonged UV irradiation, a significant contribution from the photodissociation of NO_2 was observed in the spectrum intensity of O atoms. Direct detection of NO was a supporting evidence for the secondary photoproduction of NO via NO_2^-.

Acknowledgment. M.K. and D.E.S. thank the Daiwa Adrian Foundation for funding. The Biogeochemistry Research Centre is a joint venture between the School of Chemistry and the Departments of Earth Science and Geography. The authors would like to offer special thanks to the members of ISCAT consortium for allowing use of the NO and ozone date collected during the 2000 compaign. In particular, we thank Doug Davis and Greg Huey for their correspondence, helpful discussion and for the initial data access. P.D.H. wishes to thank NERC and BAS for funding.

References and Notes

(1) Karapet'yants M. Kh.; Karapet'yants M. K. *Handbook of thermodynamic constants of inorganic and organic compounds*; Ann Arbor-

Humphrey Science Publishers, 1970. ΔH in units of kJ/mol: $HNO_3(d) = -207.4$, $HNO_3(l) = -174.1$, $NO_2^-(d) = -104.6$, $O(^3P_2)(g) = 249.2$, $O^-(d) = -50.21$, $NO_2(g) = 33.18$, $HONO = -79.50$, $HNO_3{\cdot}H_2O = -473.5$, $HNO_3{\cdot}3H_2O = -1056$, $H_2O(l) = -285.8$, $NO_3^-(d) = -207.4$, $H_3O^+(d) = -285.8$, $H(g) = 38.96$.

(2) Dubowski, Y.; Colussi, A. J.; Hoffmann, M. R. *J. Phys. Chem. A* **2001**, *105*, 4928.

(3) Dubowski, Y.; Colussi, A. J.; Boxe, C.; Hoffmann, M. R. *J. Phys. Chem. A* **2002**, *106*, 6967.

(4) Chu, L.; Anastasio, C. *J. Phys. Chem. A* **2003**, *107*, 9594.

(5) Mack, J.; Bolton, J. R. *J. Photochem. Photobiol. A* **1999**, *128*, 1.

(6) Warneck, P.; Wurzinger, C. *J. Phys. Chem.* **1988**, *92*, 6278.

(7) Mark, G.; Korth, H.-G.; Schuchmann, H.-P.; von Sonntag, C. *J. Photochem. Photobiol. A* **1996**, *101*, 89.

(8) Davis, D. D.; Nowak, J. B.; Chen, G.; Buhr, M.; Arimoto, R.; Hogan, A.; Eisele, F.; Maudlin, L.; Tanner, D.; Shetter, R.; Lefer, B.; McMurry, P. *Geophys. Res. Lett.* **2001**, *28*, 3625.

(9) Honrath, R. E.; Peterson, M. C.; Guo, S.; Dibb, J. E.; Shepson, P. B.; Campbell, B. *Geophys. Res. Lett.* **1999**, *26*, 695.

(10) Honrath, R. E.; Guo, S.; Peterson, M. C.; Dziobak, M. P.; Dibb, J. E.; Arsenault, M. A. *J. Geophys. Res.-Atmos.* **2000**, *105*, 24183.

(11) Cotter, E. S. N.; Jones, A. E.; Wolff, E. W.; Baugitte, S. J.-B. *J. Geophys. Res.-Atmos.* **2003**, *108*, 4147.

(12) Law, K. S. *Science* **2007**, *315*, 1537.

(13) Yabushita, A.; Inoue, Y.; Senga, T.; Kawasaki, M.; Sato, S. *J. Phys. Chem. B* **2002**, *106*, 3151.

(14) Kawasaki, M. *Appl. Surf. Sci.* **1998**, *135*, 1159.

(15) Sato, S.; Ymaguchi, D.; Nakagawa, K.; Inoue, Y.; Yabushita, A.; Kawasaki, M. *Langmuir* **2000**, *16*, 9533.

(16) Leu, M.-T. *Geophys. Res. Lett.* **1998**, *15*, 17.

(17) Zimmermann, F. M.; Ho, W. *Surf. Sci. Rep.* **1995**, *22*, 127.

(18) Pursell, C. J.; Everest, M. A.; Falgout, M. A.; Sanchez, D. D. *J. Phys. Chem. A.* **2002**, *106*, 7764.

(19) Senga, T.; Yabushita, A.; Inoue, Y.; Kawasaki, M.; Sato, S. *Bull. Chem. Soc. Jpn.* **2001**, *74*, 689.

(20) Hasselbrink, E.; Jakubith, S.; Nettesheim, S.; Wolf, M.; Cassuto, A.; Ertl, G. *J. Chem. Phys.* **1990**, *92*, 3154.

(21) Thibert, E.; Domine, F. *J. Phys. Chem. B.* **1998**, *102*, 4432.

(22) Yabushita, A.; Kanda, D.; Kawanaka, N.; Kawasaki, M.; Ashfold, M. N. R. *J. Chem. Phys.* **2006**, *125*, 133406.

(23) Yabushita, A.; Inoue, Y.; Senga, T.; Kawasaki, M.; Sato, S. *J. Phys. Chem. A.* **2004**, *108*, 438.

(24) Riordan, E.; Minogue, N.; Healy, D.; O'Driscoll, P.; Sodeau, J. R. *J. Phys. Chem. A.* **2005**, *109*, 779.

(25) Beine, H. J.; Amoroso, A.; Domine, F.; King, M. D.; Nardino, M.; Ianniello, A.; France, J. L. *Atmos. Chem. Phys.* **2006**, *6*, 22569.

(26) Boxe, C. S.; Colussi, A. J.; Hoffmann, M. R.; Murphy, J.; Wooldridge, P. J.; Betram, T.; Cohen, R. C. *J. Phys. Chem. A.* **2005**, 109, 8520.

(27) Boxe, C. S.; Colussi, A. J.; Hoffmann, M. R.; Perez, I. M.; Murphy, J. G.; Cohen, R. C. *J. Phys. Chem. A.* **2006**, *110*, 3578

(28) Bartels-Rausch, T.; Donaldson, D. J. *Atmos. Chem. Phys. Discuss.* **2006**, *6*, 10713.

(29) Margitan, J. J.; Watson, R. T. *J. Phys. Chem.* **1982**, *86*, 3819.

(30) Riffault, V.; Gierczak, T.; Burkholder, J. B.; Ravishankara, A. R. *Phys. Chem. Chem. Phys.* **2006**, *8*, 1079.

(31) Weller, R.; Minikin, A.; Konig-Langlo, G.; Schrems, O.; Jones, A. E.; Wolff, E. W.; Anderson, P. S. *Geophys. Res. Lett.* **1999**, *26*, 2853.

(32) Jones, A. E.; Weller, R.; Minikin, A.; Wolff, E. W.; Sturges, W. T.; McIntyre, H. P.; Leonard, S. R.; Schrems, O.; Bauguitte, S. *J. Geophys. Res.-Atmos.* **1999**, *104*, 21355.

(33) Jones, A. E.; Wolff, E. W. *J. Geophys. Res.-Atmos.* **2003**, *108*, 4565.

(34) Dominé, F.; Shepson, F. P. B. *Science* **2002**, *297*, 1506.

(35) Jones, A. E.; Weller, R.; Wolff, E. W.; Jacobi, H. W. *Geophys. Res. Lett.* **2000**, *27*, 345.

(36) Crawford, J. H.; Davis, D. D.; Chen, G.; Buhr, M.; Oltmans, S.; Weller, R.; Maudlin, L.; Eisele, F.; Shetter, R.; Lefer, B.; Arimoto, R.; Hogan, A. *Geophys. Res. Lett.* **2001**, *28*, 3641.

(37) Hamer, P. D.; Shallcross, D. E. *Atmos. Sci. Lett.* **2007**, *8*, 14.

(38) Oncley, S. P.; Buhr, M.; Lenschow, D. H.; Davis, D.; Semmer, S. R. *Atmos. Environ.* **2004**, *38*, 5389.

(39) Davis, D. D. personal communication.

(40) Browell, E. V.; Hair, J. W.; Butler, C. F.; Grant, W. B.; DeYoung, R. J.; Fenn, M. A.; Brackett, V. G.; Clayton, M. B.; Brasseur, L. A.; Harper, D. B.; Ridley, B. A.; Klonecki, A. A.; Hess, P. G.; Emmons, L. K.; Tie, X. X.; Atlas, E. L.; Cantrell, C. A.; Wimmers, A. J.; Blake, D. R.; Coffey, M. T.; Hannigan, J. W.; Dibb, J. E; Talbot, R. W.; Flocke, F.; Weinheimer, A. J.; Fried, A.; Wert, B.; Snow, J. A.; Lefer, B. L. *J. Geophys. Res.-Atmos.* **2003**, *108*, 8369.

(41) Stroud, C.; Madronich, S.; Atlas, E.; Ridley, B.; Flocke, F.; Weinheimer, A.; Talbot, B.; Fried, A.; Wert, B.; Shetter, R.; Lefer, B.; Coffey, M.; Heikes, B.; Blake, D. *Atmos. Environ.* **2003**, *37*, 3351.

(42) Emmons, L. K.; Hess, P.; Klonecki, A.; Tie, X.; Horowitz, L.; Lamarque, J. F.; Kinnison, D.; Brasseur, G.; Atlas, E.; Browell, E.; Cantrell, C.; Eisele, F.; Mauldin, R. L.; Merrill, J.; Ridley, B.; Shetter, R. *J. Geophys. Res.-Atmos.* **2003**, *108*, 8372.

(43) Oltmans, S. J.; Lefohn, A. S.; Harris, J. M.; Galbally, I.; Scheel, H. E.; Bodeker, G.; Brunke, E.; Claude, H.; Tarasick, D.; Johnson, B. J.; Simmonds, P.; Shadwick, D.; Anlauf, K.; Hayden, K.; Schmidlin, F.; Fujimoto, T.; Akagi, K.; Meyer, C.; Nichol, S.; Davies, J.; Redondas, A.; Cuevas, E. *Atmos. Environ.* **2006**, *40*, 3156.

(44) Penkett, S. A.; Brice, K. A. *Nature* **1986**, *319*, 655.

(45) Stroud, C.; Madronich, S.; Atlas, E.; Ridley, B.; Flocke, F.; Weinheimer, A.; Talbot, B.; Fried, A.; Wert, B.; Shetter, R.; Lefer, B.; Coffey, M.; Heikes, B.; Blake, D. *Atmos. Environ.* **2003**, *37*, 3351.

(46) Beyersdorf, A. J.; Blake, N. J.; Swanson, A. L.; Meinardi, S.; Dibb, J. E.; Sjostedt, S.; Huey, G.; Lefer, B.; Rowland, F. S.; Blake, D. R. *Atmos. Environ.* In press.